ChemComm

Accepted Manuscript

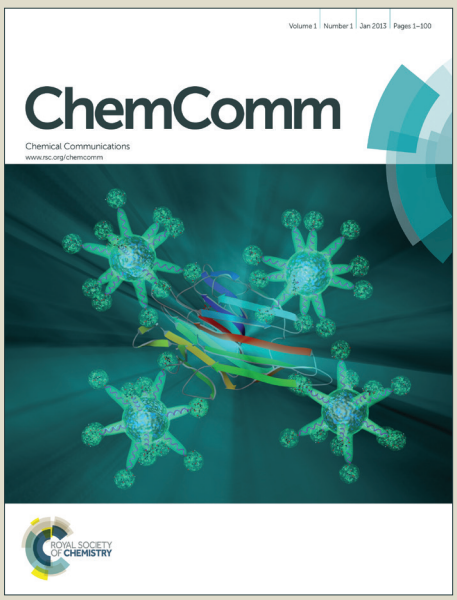

This is an *Accepted Manuscript*, which has been through the Royal Society of Chemistry peer review process and has been accepted for publication.

Accepted Manuscripts are published online shortly after acceptance, before technical editing, formatting and proof reading. Using this free service, authors can make their results available to the community, in citable form, before we publish the edited article. We will replace this *Accepted Manuscript* with the edited and formatted *Advance Article* as soon as it is available.

You can find more information about *Accepted Manuscripts* in the Information for Authors.

Please note that technical editing may introduce minor changes to the text and/or graphics, which may alter content. The journal's standard Terms & Conditions and the Ethical guidelines still apply. In no event shall the Royal Society of Chemistry be held responsible for any errors or omissions in this *Accepted Manuscript* or any consequences arising from the use of any information it contains.

ROYAL SOCIETY OF CHEMISTRY

www.rsc.org/chemcomm

Journal Name

RSCPublishing

COMMUNICATION

Electrical conductivity in p-type BiOCl nanosheets

Cite this: DOI: 10.1039/x0xx00000x

Yoon Myung,[a] Fei Wu,[a] Sriya Banerjee,[a] Jeunghee Park,[b] and Parag Banerjee[a*]

Received 00th January 2012,
Accepted 00th January 2012

DOI: 10.1039/x0xx00000x

www.rsc.org/

High quality BiOCl nanosheets were fabricated using facile, room temperature hydrolysis of $Bi(NO_3)_3$ and HCl. The resulting nanosheets had dimensions of 500 nm with exposed {001} facet. The band gap of the nanosheets was found to be 3.34 eV with conduction and valence band edges at -3.63 eV and -6.97 eV with respect to vacuum, respectively. The electrical conductivity of drop-cast BiOCl nanosheets were measured between aluminum patterned electrodes as a function of temperature and oxygen partial pressure (pO_2). The activation energy for conduction in BiOCl was found to be 862 meV in the temperature range of 300 K – 425 K and under 1000 mbar. The electrical conductivity varied with pO_2, indicating $\sigma \propto pO_2^{1/4.05}$ and $\sigma \propto pO_2^{1/32}$ for low and sub atmospheric pressures, respectively. A prototypical device for low temperature (425 K) O_2 sensing was demonstrated.

BiOCl is a V-VI-VII ternary compound semiconductor that has attracted increasing attention due to its unique optical, electrical and catalytic properties. The matlockite (PbFCl) type structure (space group D^7_{4h}-P4/nmm) of BiOCl consists of alternatively stacked layers of $[Bi_2O_2]^{2+}$ slabs between two sheets of Cl^- ions along the c-axis.[1] This charged layered structure creates internal dipole moments that can increase electron-hole separation.[2] Furthermore, BiOCl is a wide band-gap (~ 3.4 eV) *p*-type semiconductor with band edges sufficiently high to create large over-potentials for driving electron transfer (reduction) reactions.[3] Because of this, BiOCl is being exploited as photocatalysts[4], photoelectrochemical cell[5], chloride ion battery[6], and as gas sensors.[7]

To prepare highly efficient BiOCl targeting the above applications, synthesis schemes which create high surface area nanostructures, such as nanosheets[8], nanoflowers[9], nanospheres[10], and nanowires[11] have been devised. These nanostructures provide large optical path lengths for photon absorption and relatively short diffusion lengths for charge transport to surface sites where finally, charge transfer reactions can efficiently occur. While charge transfer reactions on the surface of BiOCl have been studied, the intrinsic, charge transport mechanism in BiOCl has not received much attention.[12] Till date, Shtilikha et al.,[13] reported thermal conductivity of BiOCl, measured between 90 and 300 K. The electronic component of heat conductivity was negligible and thus, it was speculated that BiOCl acts as an insulator (conductivity $\propto 10^{-10} – 10^{-13}\ \Omega^{-1}\cdot cm^{-1}$).

In this paper, we synthesize BiOCl nanosheets by a facile, hydrolysis method and report on the electrical conductivity as a function of temperature and oxygen partial pressure (pO_2). We find that the nanosheets are pristine and single crystalline and that their conductivity behavior is highly dependent on pO_2. This allows us to create a prototypical O_2 sensor which is optimized to run at 425 K but can work at temperatures as low as 380 K.

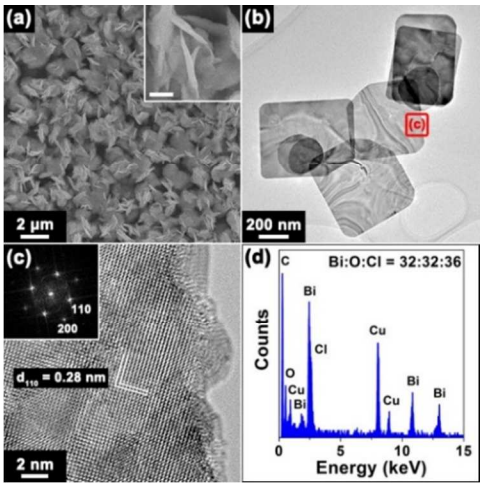

Fig. 1 SEM image showing the general morphology of BiOCl nanosheets synthesized using hydrolysis method. (inset) magnified image with scale bar represents 300 nm (b) TEM image of individual BiOCl nanosheets, (c) lattice resolved image of BiOCl nanosheet. The insets represent FFT-ED patterns and (d) their EDX data.

ChemComm Accepted Manuscript

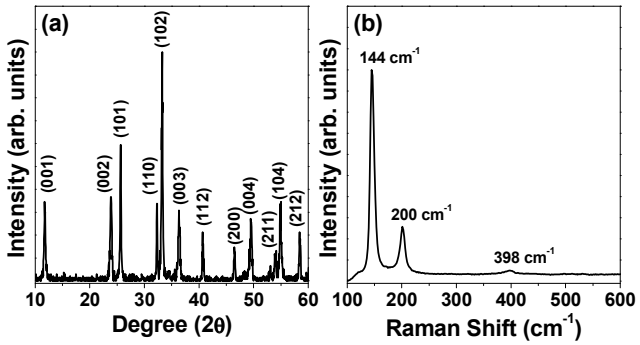

Fig. 2 (a) XRD pattern and (b) Raman spectra of BiOCl nanosheets. No impurity phases were detected.

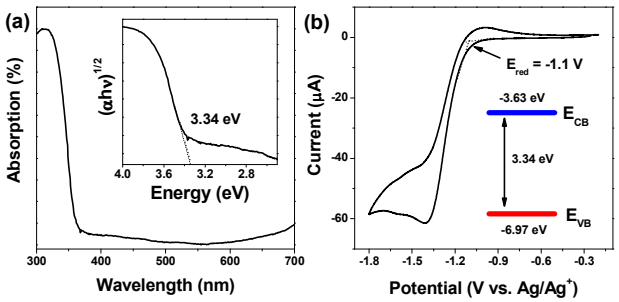

Fig. 3 (a) UV-visible absorption spectra of BiOCl nanosheets and (inset) plot of (ahn)1/2 vesus photon energy. (b) CV curve (vs Ag/Ag^+ reference electrode) of BiOCl nanosheets. The inset shows scheme of band position of BiOCl.

The detailed experimental procedure is described in Electronic Supplementary Information (ESI).

The shape and morphology of the as-synthesized nanosheets was confirmed by FE-SEM. As shown in Fig. 1a, the BiOCl consisted of homogeneous, nanosheet shaped structures with an average thicknesses of 80 nm. The low magnification FE-TEM image (Fig. 1b) exhibits the individual nanosheets with average size of 500 nm. Each individual sheet is single crystalline and no presence of grain boundaries is observed. Fig. 1c shows the lattice resolved image of the nanosheet. Clear fringes of lattices with a d-spacing of 0.28 nm is noted. This is consistent with BiOCl (110) planes of reference (JCPDS No. 85-0861; *a*=3.890 Å, *c*=7.370 Å). A corresponding FFT-ED pattern (Fig. 1c, inset) generated by high resolution (HR) TEM image could be indexed to the (110) and (200) planes of the tetragonal system of BiOCl. Thus, the surface facets of the nanosheet are exposed to {001} and side facets were composed of {110}. These results are well-matched with previously reported, facet controlled, BiOCl nanosheets under low (< 6) pH conditions.[12] The energy dispersive x-ray spectroscopy (EDX) of this nanosheet also indicates that Bi, O, and Cl are the main elements with atomic percentage of Bi/O/Cl was 32:32:36, i.e., close to 1:1:1 (Fig.1d).

It is well known that $Bi(NO_3)_3$ can be hydrolyzed immediately in water with HCl to form BiOCl compound due to the low solubility product (K_{sp}) of BiOCl (1.8×10^{-31}).[14]

$$Bi(NO_3)_3 + HCl + H_2O \rightarrow BiOCl\downarrow + 3HNO_3$$

Based on the above chemical reaction, as the pH value of the solution is lowered (due to HNO_3 formation), BiOCl initially dissolves in the acidic solution. When DI water is added, the pH increases, causing the nucleation and growth of the BiOCl along the {001} facet, which is terminated with a high density of oxygen atoms.[15] This results in the turbidity observed when DI water is added back into the solution.

XRD pattern of BiOCl is shown in Fig. 2a. All peaks can be indexed to the tetragonal BiOCl according to the reference (JCPDS No. 85-0861; *a*=3.890 Å, *c*=7.370 Å). There are no impurity phases present. The Raman spectrum of the BiOCl nanosheets is shown in Fig. 2b. The significantly strong band at 144 cm^{-1} is assigned to the A_{1g} internal Bi-Cl stretching mode in BiOCl. The band at 200 cm^{-1} is attributed to the E_g internal Bi-Cl stretching mode, while the E_g external Bi-Cl stretching is masked by the strong Raman band at 144 cm^{-1}. The weak band at 398 cm^{-1} arises from the motion of oxygen atoms produced by E_g and B_{1g} band stretching. All the peak positions are well-matched with reported values in literature.[16]

Fig. 3a shows the diffuse reflectance spectra of BiOCl nanosheets. It shows the single absorption edge near 360 nm, indicating the presence of BiOCl. The spectra was also used to estimate the band (indirect) gap by performing the Kubelka-Munk transformation.[17] A plot of $[\alpha h\nu]^{1/2}$ (where α is the absorption coefficient) versus photon energy yield a band gap of 3.34 eV. This result is consistent with the value from previous reports on BiOCl.[18] For more detailed understanding of band edge positions of BiOCl nanosheets, we measured CV using a scan rate of 20 mV/s.

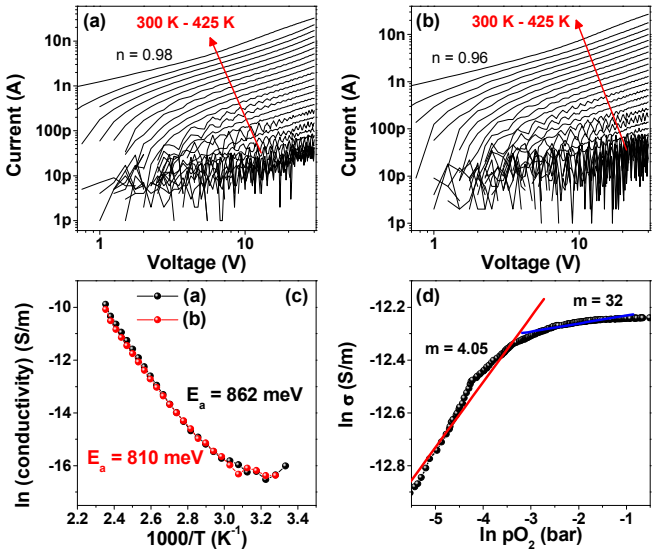

Fig. 4 Temperature dependent I-V characteristics (log-log scale) of BiOCl nanosheet electrode between 300 and 425 K at (a) 1000 mbar and (b) 3 mbar. The slope of both the graphs ('n') is close to 1. (c) Arrhenius plot of conductivity versus reciprocal temperature yields the activation energy for Ea = 862 meV and (b) 810 meV, respectively. (d) plots of ln conductivity versus ln oxygen partial pressure of BiOCl nanosheet electrode at 425 K under applied bias at 30V.

ChemComm Accepted Manuscript

This journal is © The Royal Society of Chemistry 2012

As shown in Fig. 3b, the reduction peak edge at -1.1 V for the BiOCl was estimated to be the conduction band position, E_{CB} = -3.63 eV, whereas valence band position was calculated to E_{VB} = -6.97 eV. The values are consistent with BiOCl band edges reported in literature.[5]

The electrical transport properties of BiOCl nanosheet films were measured by a two point probe configuration as a function of temperature and pO_2. We note that four point probe resistivity measurements are the preferred form for obtaining resistivity values of materials. However in our case, attempts to conduct four point probe measurements resulted in cracking of the dried and particulate film as the four probes touched the BiOCl surface. Better test structure designs will be created to counter cracking in the future. For now, we present our two-point probe measurements which assume special significance, given that the electrical conductivity in BiOCl has never been explored previously (see ESI Fig. SI1 for detailed electrode scheme).

Fig. 4a shows the current-voltage (I-V) characteristics of drop-cast BiOCl nanosheets films in 1000 mbar oxygen atmosphere condition. As expected of a semiconductor, increasing temperature leads to increase in the conductivity by a factor of ~450 in the temperature range of 300 K to 425 K. Thus for example, the resistance of BiOCl at 300 K is given as 750 GΩ whereas at 425 K the resistance is 0.93 GΩ at 30V, respectively.

Under low pressure (3 mbar) (Fig. 4b), the current decreased. For example, the maximum current at 425 K decreased by a factor of ~540. Additionally, log-log I-V plotting shows a slope ('n' in Fig. 4a, b) of ~1 for all I-V curves that indicates linear, ohmic conduction in the temperature regime tested. Generally, the relationship of activation energy and conductivity (σ) can be expressed as an Arrhenius equation.[19]

$$\sigma = \sigma_0 \cdot \exp(-E_a/k_B \cdot T)$$

Where σ_0 pre-exponential factor, E_a is activation energy, k_B is the Boltzmann constant, and T is temperature in Kelvin. As seen in Fig. 4c, the slope of ln (conductivity) as a function of 1000/T yields E_a, which was 862 meV for the I-V at 1000 mbar, and 810 meV for the 3 mbar, for the temperature range 300 K - 425 K, respectively.

The conductivity dependency on oxygen partial pressure can be expressed by the following equation.[20]

$$\sigma = K(T) \cdot pO_2^{1/m}$$

where, K(T) is a function of temperature, and m is a constant. Fig. 4d shows ln(conductivity) vs. ln(pO_2) to calculate pO_2 dependency of BiOCl nanosheets at 425 K with an applied bias of 30 V.

Two observations can be made from this graph. First, the *p*-type characteristic, where conductivity decreases with decreasing pO_2, is clearly observed. Second, the slope of the pO_2 dependent conductivity is seen to vary as a function of pO_2. To analyze this further, the region is split into two pressure ranges; 1) In the range of 371 mbar to 48 mbar and 2) from 48 mbar to 3 mbar. In the 371 mbar to 48 mbar region, the oxygen partial pressure dependence is proportional to $pO_2^{1/32}$. In contrast, the lower oxygen partial pressure region is proportional to $pO_2^{1/4.05}$. We note here that in pure oxides, an m = 4 represents electronic conductivity dependence on single charge oxygen vacancies ($V_O^{\bullet}$), whereas for m = 6, the conductivity depends on doubly charged oxygen vacancies ($V_O^{\bullet\bullet}$).[21]

Generally, compound semiconductors and oxides possesses intrinsic defects such as metal cationic vacancy (V_M^{n-}, where *n* is the charge on the cation and we use the Kröger-Vink notation) and oxygen interstitials (O_i''). The presence of these defects is known to generate electrons and holes and thus, impact conductivity beyond what is intrinsically observed. For example, the presence of oxygen vacancy ($V_O^{\bullet\bullet}$) can release 2 electrons to the BiOCl, thereby compensating holes and making BiOCl less conducting.[21] It has been shown that BiOCl possess intrinsic defects including $V_O^{\bullet\bullet}$, bismuth vacancy (V_{Bi}''') and triple associated vacancy of $V_{Bi}'''V_O^{\bullet\bullet}V_{Bi}'''$.[22] While the defect reactions and their partial pressure dependencies need to be investigated fully, we speculate that under higher pressures, closer to ambient (371 mbar to 48 mbar) when O loss is less, the concentration of $V_O^{\bullet\bullet}$ may be low and therefore, $V_O^{\bullet\bullet}$ may be stabilized by the association with V_{Bi}''', thus leading to the formation of the triplet vacancy. This could explain the weak m = 32 dependency.

Alternatively, under low pressures (48 mbar to 3 mbar), when O loss is significant, the concentration of singly or doubly charged oxygen vacancy, $V_O^{\bullet}$ or $V_O^{\bullet\bullet}$ increases and this could lead to the existence of the defects without association with V_{Bi}'''. This could explain the stronger, m = 4.05 behavior. We note that given 1) the relative independence of activation energy (862 meV vs. 810 meV) on pO_2, 2) large activation energy for conduction observed, the role of ionic conductivity is not ruled out and needs to be explored further.

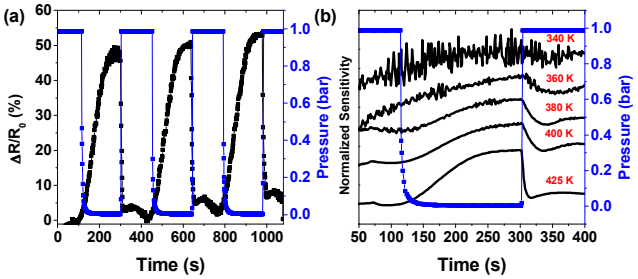

Fig. 5 Resistance changes ($\triangle R/R_0$) of the BiOCl nanosheets electrode upon its exposure to oxygen and (b) their temperature dependent response. Blue curve represents pressure change as a function of time.

Finally, we measure the ability of the BiOCl nanosheets to be used as a gas sensor under an applied bias of 30 V at 425 K. Fig. 5a displays the relative resistance change ($\Delta R/R_o$) as a function of chamber pressure. The drop cast nanosheets show promising response as dry air is removed and purged into the system. The $\Delta R/R_o$ reaches 50% as chamber pressure changes from 1000 mbar to 3 mbar and vice versa. This indicates that O removal and insertion in the BiOCl nanosheets is reversible and repeatable. ESI, Fig SI2 contains detailed response changes under various oxygen partial pressure. These response features are well matched with their conductivity dependence and show that under low pressures, conductivity change depends on oxygen partial pressure while over 17 mbar it shows saturated

ChemComm Accepted Manuscript

behavior. Fig. 5b shows temperature dependency of the O response of BiOCl nanosheet electrodes. Here the temperature is varied as 340 K, 360 K, 380 K, 400 K and 425 K. BiOCl nanosheets show no gas response until 340 K. At 360 K (i.e., 87 °C), a gradually increase and decrease in current is seen and the recovery time is ~60 seconds. At 425 K however, the recovery time is reduced to 15 seconds. Therefore, BiOCl nanosheets shows promise to be used as a low temperature, reliable O_2 sensor.

In summary, BiOCl nanosheets were synthesized by a facile hydrolysis method. The nanosheets consisted of single crystalline BiOCl with dominant {001} facet and average size of 500 nm. The UV-vis and CV measurements confirm that the conduction band position and valence band position are -3.63 eV and -6.97 eV with respect to vacuum, respectively. The charge transport measurements demonstrate that BiOCl has *p*-type semiconducting characteristics. The activation energy of conductivity is found to be 862 meV for temperatures between 300 K – 425 K and under 1000 mbar pressure. The conductivity behavior of BiOCl as a function of pO_2 is investigated. Under sub-atmospheric conditions, we suggest an associated triplet defect could reduce conductivity dependency on pO_2, whereas under low vacuum, singly charged oxygen vacancy could be responsible for releasing electrons and reducing conductivity even further. A prototypical O_2 gas sensor is demonstrated in this work.

Support for this work comes from the International Center for Advanced Renewable Energy and Sustainability (I-CARES) and start–up funds from Washington University. Partial funding from the McDonnell Academy Global Energy and Environment Partnership (MAGEEP) is acknowledged. Microscopy work at the JENS lab at Washington University is acknowledged. XRD was obtained at the Microprobe & XRD facility of the Earth & Planetary Sciences Laboratory at Washington University. Diffused reflectance data was obtained in the Aerosol and Air-Quality Research Lab. Raman Microscopy data was obtained in the Soft Nanomaterials Lab.

Notes and references

[a] Department of Mechanical Engineering and Materials Science, Washington University in St. Louis, St. Louis, MO 63130, USA
[b] Department of Chemistry, Korea University, Jochiwon 339-700, Korea
* Corresponding author, e-mail: parag.banerjee@wustl.edu
Electronic Supplementary Information (ESI) available: Experimental details, electrode scheme and oxygen response curves. See DOI: 10.1039/c000000x/

1(a) L. Armelao, G. Bottaro, C. Maccato and E. Tondello, *Dalton Transactions*, 2012, **41**, 5480; (b) H. F. Cheng, B. B. Huang and Y. Dai, *Nanoscale*, 2014, **6**, 2009.
2 J. Li, Y. Yu and L. Z. Zhang, *Nanoscale*, 2014, **6**, 8473.
3 L. Kong, Z. Jiang, H. H. C. Lai, T. Xiao and P. P. Edwards, *Progress in Natural Science-Materials International*, 2013, **23**, 286.
4 L. Ye, K. Deng, F. Xu, L. Tian, T. Peng and L. Zan, *Physical Chemistry Chemical Physics*, 2012, **14**, 82.
5 S. Weng, B. Chen, L. Xie, Z. Zheng and P. Liu, *Journal of Materials Chemistry A*, 2013, **1**, 3068.
6 X. Y. Zhao, Z. Zhao-Karger, D. Wang and M. Fichtner, *Angew. Chem.-Int. Edit.*, 2013, **52**, 13621.
7(a) C. R. Michel, N. L. L. Contreras and A. H. Martinez-Preciado, *Sens. Actuator B-Chem.*, 2012, **173**, 100; (b) *Sens. Actuator B-Chem.*, 2011, **160**, 271.
8 L. Ye, L. Zan, L. Tian, T. Peng and J. Zhang, *Chemical Communications*, 2011, **47**, 6951.
9 S. Cao, C. Guo, Y. Lv, Y. Guo and Q. Liu, *Nanotechnology*, 2009, **20**.
10 X. Zhang, Z. Ai, F. Jia and L. Zhang, *Journal of Physical Chemistry C*, 2008, **112**, 747.
11 S. Wu, C. Wang, Y. Cui, T. Wang, B. Huang, X. Zhang, X. Qin and P. Brault, *Materials Letters*, 2010, **64**, 115.
12 J. Jiang, K. Zhao, X. Y. Xiao and L. Z. Zhang, *Journal of the American Chemical Society*, 2012, **134**, 4473.
13 M. V. Shtilikha and D. V. Chepur, *Sov. Phys.-Solid State*, 1972, **14**, 1354.
14 J. Geng, W. H. Hou, Y. N. Lv, J. J. Zhu and H. Y. Chen, *Inorg. Chem.*, 2005, **44**, 8503.
15 K. Zhao, L. Z. Zhang, J. J. Wang, Q. X. Li, W. W. He and J. J. Yin, *Journal of the American Chemical Society*, 2013, **135**, 15750.
16 J. Y. Xiong, G. Cheng, G. F. Li, F. Qin and R. Chen, *RSC Adv.*, 2011, **1**, 1542.
17 D. D. Vaughn, R. J. Patel, M. A. Hickner and R. E. Schaak, *Journal of the American Chemical Society*, 2010, **132**, 15170.
18 Y. Y. Li, J. P. Liu, J. Jiang and J. G. Yu, *Dalton Transactions*, 2011, **40**, 6632.
19 Y. X. Liu, J. Parisi, X. C. Sun and Y. Lei, *Journal of Materials Chemistry A*, 2014, **2**, 9919.
20 C. Kevane, *Physical Review*, 1964, **133**, A1431.
21 D. M. Smyth, *The Defect Chemistry of Metal Oxides, by DM Smyth, pp. 304. Foreword by DM Smyth. Oxford University Press, Jun 2000. ISBN-10: 0195110145. ISBN-13: 9780195110142*, 2000, **1**.
22(a) M. Guan, C. Xiao, J. Zhang, S. Fan, R. An, Q. Cheng, J. Xie, M. Zhou, B. Ye and Y. Xie, *Journal of the American Chemical Society*, 2013, **135**, 10411; (b) H. Li and L. Z. Zhang, *Nanoscale*, 2014, **6**, 7805.

Table of Content

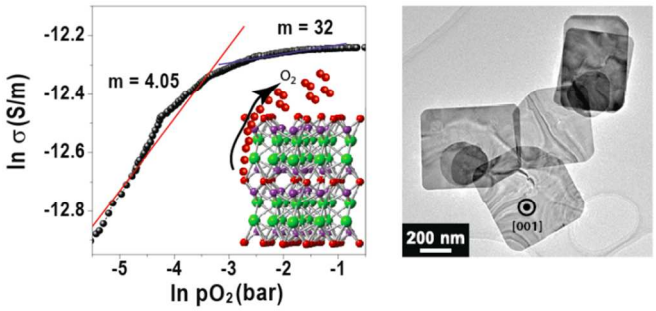

BiOCl nanosheets was synthesized using a facile hydrolysis method and was measured their p-type electrical conduction as a function of oxygen partial pressure.

ChemComm Accepted Manuscript

This journal is © The Royal Society of Chemistry 2012